Research Square

Preprints are preliminary reports that have not undergone peer review.
They should not be considered conclusive, used to inform clinical practice,
or referenced by the media as validated information.

The Mechanism Revealing and Law Explorating for the Nonlinear Response of Blade Disk Rotor System Under the Coupling Effects of Crack and Aerodynamic Force

Jinsong Yang
Central South University
Jingsong Xie (jingsongxie@foxmail.com)
Central South University
Tiantian Wang
Central South University
Fei Yang
Kunming Institute of Physics
Jinglong Chen
Xi’an Jiaotong University

Research Article

Keywords: Blade disk rotor system, industrial equipments, aeroengines , gas turbines

Posted Date: September 27th, 2021

DOI: https://doi.org/10.21203/rs.3.rs-900158/v1

License: This work is licensed under a Creative Commons Attribution 4.0 International License.
Read Full License

The mechanism revealing and law explorating for the nonlinear response of blade disk rotor system under the coupling effects of crack and aerodynamic force

J. Yang[1], J. Xie[1*], T. Wang[1], F. Yang[2], and J. Chen[3]

[1] School of Traffic and Transportation Engineering, Central South University, Changsha, 410075 P. R. China
[2] Kunming Institute of Physics, Kunming, 650000, P. R. China

[3] State Key Laboratory for Manufacturing Systems Engineering, Xi'an Jiaotong University, Xi'an, 710049, P. R. China.

Corresponding author: J. Xie (e-mail: jingsongxie@foxmail.com)

Abstract

Blade disk rotor system is a typical structure of industrial equipments such as aeroengines and gas turbines. The research on the response characteristics and mechanism of the system under the coupling effects of aerodynamic force and blade crack is of great significance to the interpretation of vibration phenomena and diagnosis of faults. From the numerical solution based response characteristic analysis to the kinematics and dynamics based essential response mechanism revealing, from the model based special case study to the Number Theory based general law establishing, in this paper, the response mechanism of blade disk rotor system under the coupling effects of crack and aerodynamic force is studied comprehensively and deeply. Firstly, a simplified dynamic model of typical blade disk rotor system is constructed by using the classical continuous parameter modeling method. Based on the dynamic model, for two structural forms of moving and stationary blades, the typical characteristics of vibration response under the actions of aerodynamic force and blade crack are analyzed by means of numerical solution. Then, from the perspective of kinematics and dynamics, the internal mechanism between the vibration responses and the excitations are revealed. Finally, based on Number Theory, the response characteristics and mechanism of typical structures are summarized, and the general laws of responses with general structural forms are established.

Introduction

The mechanism of vibration response characteristics and fault characteristics is the key priori information for equipment vibration phenomenon analysis, health assessment and fault diagnosis. Therefore, the revelation of vibration response mechanism has been a basic scientific problem that experts have been committed to solving for a long time. After continuous research, scholars have comprehensively and accurately revealed the vibration characteristics and response mechanism of key parts such as shafts, bearings and gears, etc.

The vibration characteristics of amplitude and phase are used to detect the unbalance of the rotor system [1]. According to the characteristics and mechanism of the rotor unbalance, in order to suppress the rotor vibration caused by the unbalance, an active control method using a magnetic actuator is proposed [2]. Xie [3, 4] discovered a new modulation frequency characteristic under the disturbance state of the cracked rotor system, and explained the modulation mechanism. The instantaneous whirling speed of is defined, and its response mechanism is revealed. Through dynamic analysis and experimental research, the mechanism of torsional vibration characteristics of cracked and non cracked rotor systems is discussed [5]. Li [6] used the zero stress intensity factor method to solve the stiffness of the rotor system with slant cracks, and studied the effects of fractional order, speed and crack depth on the dynamic characteristics of the rotor system. The rotating orbit, time domain response and spectrum are obtained to show the phenomenon of superharmonic resonance in the hollow shaft cracked rotor system [7]. Cao [8] discussed the contact characteristics between a roller and race ways and the changes of roller rotation angular speed. Xiang [9] proposed a nonlinear dynamic model of bearing based on collision system to simulate the vibration characteristics of different fault types. Guo [10] proposed a new dynamic model and studied the double pulse behavior and mechanism of bearing raceway surface spallation. Bachar [11] studied the influence of working conditions and surface roughness on the vibration characteristics of spur gear transmission, and studied the detection ability of single tooth surface fault. Chen [12] analyzed the changes of dynamic response in time domain and frequency domain for different wear degrees at tooth surface. Yang [13] revealed the variation law of time-varying meshing stiffness, the time history and frequency spectrum of vibration signal under chipping damage. Cao [14] discussed the effects of external load and damping parameters on frequency response and force response curve by using the equivalent nonlinear model of nonlinear beam truss.

The above research of mechanism revealing has significantly promoted the mastery of the vibration law of key parts. Based on this, many reliable and accurate fault diagnosis methods have been established, which has important theoretical significance and economic value.

The blade disk rotor system is different from the above typical parts, which is composed of shaft, disk and multiple blades. Scholars have studied the vibration characteristics and mechanism from the aspects of single blade, blade-disk system, blade-disk-rotor system, respectively.

Wu [15] indicated that when the excitation frequency changes from 0 to the first resonance frequency of a cracked beam, the crack breathing frequency increases linearly, and the crack breathing frequency changes nonlinearly with the further increase of the excitation frequency. Yang [16,17] found that severe cracks are expected to seriously reduce the stiffness of rotating blades and significantly reduce the resonance frequency. Li [18] investigated of the effects of thickness-taper ratio, pre-twist angle, rotational speed, and connection stiffness on blades modal characteristics. Zi [19] indicated that the complexity of natural frequency and forced response depends on the length and relative position of cracks. When cracks or detuning occur in the impeller, the response amplitude of the blade fluctuates periodically with the number of blades. Joachim [20] evaluated the effect of small detuning on the vibration amplitude of a 2D blade disk. Heydari [21] studied the effects of blade stagger angle and pretwist angle on shaft bending and blade bending coupling vibration. Jin [22] revealed the nonlinear vibration characteristics caused by blade-casing rubbings of a real dual rotor aeroengine. Ma [23, 24] showed that the original hardening type nonlinearity may be enhanced or transformed into softening type due to the nonlinear stiffness of the bearing and the rubbing dynamic responses of shaft-blisk-casing system at different speeds, disc imbalance, disc position and speed are solved. Liu [25] studied the dynamic behavior of casing acceleration of the whole aeroengine from the aspect of blade-casing rubbing fault diagnosis.Wei [26] showed that under the excitation of blade loss load, the transient response of the system has obvious impact characteristics, and the stiffness and damping of the rear bearing of the fan have a significant impact on the transient response. Zhao [27, 28] used the elastic supported coupling finite element model to study the rubbing of the mistuned blade disk system with variable thickness blades, and showed that the cracks significantly exacerbated the vibration of the blades. A large number of research results have been obtained in the characteristic analysis of blade disk rotor system. However, the current research shows that different structures have different characteristics, the universality law has not been established, and the deeper mechanical essence mechanism between characteristics and excitation is not clear.

It is of great significance and great challenge to analyze the essential mechanism and establish the general law of response characteristics of the bladed disk rotor system under typical excitation. In this paper, some of the work will be carried out tentatively, and only the response mechanism and law of circularly symmetric bladed disk rotor system (Structural detuning is not considered) under the coupling effects of aerodynamic force and crack will be studied.

This paper is arranged as follows. A simplified dynamic model of typical blade disk rotor system is constructed in Section 2 to provide the basis for response characteristic analysis. The typical characteristics of vibration response under aerodynamic load and blade crack for two structural forms are analyzed in Section 3. Finally, Section 4, the response characteristics and mechanism of typical structures are summarized, and general laws with general structural forms are obtained. The conclusions are drawn in Section 5.

1. Vibration model of blade disk rotor system

This paper focuses on the response characteristics and response mechanism of the blade disk rotor system excited by the aerodynamic force between the moving and stationary blades and the stiffness parametric excitation of the blade cracks. Therefore, the model construction in this section adopts the common and classical continuous parameter modeling method to establish a simplified vibration model of single-stage blade disk rotor system. The aerodynamic excitation between moving and stationary blades is simulated by typical traveling waves, and the stiffness parameter excitation of crack is simulated by the stiffness breathing function published in our last paper.

1.1 Modeling of normal system

Continuous parameter modeling method has been a common and mature modeling method, which has been widely used by scholars [25, 29, 30]. Based on this method, we have established the vibration model of a single-stage and a three-stage blade disk rotor system in our recent publications [31, 32]. Therefore, for the simplified model of single-stage blade disk rotor system required in this paper, we will not give the proof of the formula in detail, but only introduce the basic process of modeling.

1.1.1 Geometric model

The schematic diagram of blade disk shaft system is shown in Figure 1, containing a bending and torsional shaft, one disk, and some flexible blades fixed onto the outer edge of the disk with a setting angle β. $0xyz$ denotes the global coordinate, $Px_1y_1z_1$ is the rotating coordinate attached to the disk with a rotational speed Ω. h_d and h_b are the thickness of disk and blade respectively.

Under the condition of small deformation, the motion of the blade-disk-shaft system can be decomposed on three planes (*oxy, ozx, ozy*) , as shown in Figure 2 and Figure 3. The decomposed view in *ozy* plane is similar to Figure 2 and is omitted here. The thick line represents the rigid body displacement of the component , and the dashed line represents the elastic deformations of the components.

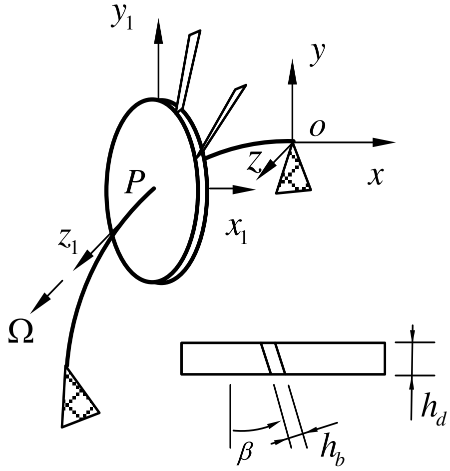

Figure 1: Schematic diagram of multistage bladed disk rotor system.

Figure 2 is the schematic diagram of the motion decomposition in *ozx* plane. Q is an arbitrary micro-unit in the disk. $w(r,\theta,t)$ represents the deflection corresponding to position (r,θ) , and (r,θ) is the local polar coordinate system fixed in the disk. $u_x(z,t)$ denotes the deflection of the shaft in x-direction. $\frac{\partial u_x(z_d,t)}{\partial z}$ is the swing angle of cross-section of the shaft at z_d. $w\left(r_2,\theta_{bi},t\right)$ is the deflection corresponding to the i^{th} blade, where r_2 presents the external diameter of the disk and θ_{bi} presents the reference angle of the i^{th} blade. $\frac{\partial w\left(r_2,\theta_{bi},t\right)}{\partial r}$ is the dip angle corresponding to the i^{th} blade. $v(l,t)\sin\left(\beta\right)$ denotes the out-plane deflection of blades.

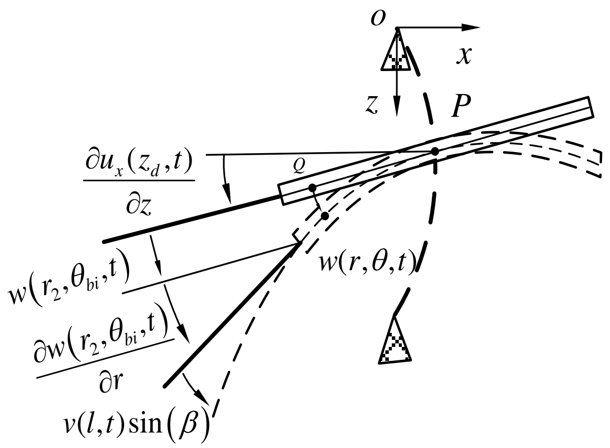

Figure 2: Decomposition of motion in *ozx* plane.

Figure 3 is the schematic diagram of the decomposition of motion in *oxy* plane. *D* is an arbitrary micro-unit in the blade and its distance from the root of the blade is *l*. *L* is the length of the blade. The direction of the x_1-axis is coincident with the spanwise direction of the reference blade (the first blade). r_1 and r_2 are the inner diameter and outer diameter of the disk respectively. $\phi(z_d,t)$ denotes the torsional displacement of shaft. $v(l,t)\cos(\beta)$ denotes the in-plane deflection of blade.

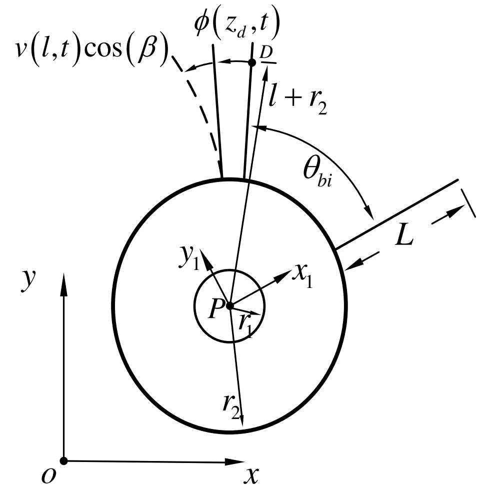

Figure 3: Decomposition of motion in *oxy* plane.

According to the above motion decompositions and coordinate system settings, during the rotation of the shaft and the elastic vibrations of structures, the coordinates of arbitrary micro-unit in the shaft with respect to the fixed coordinate system are $u=\left(u_x(z),u_y(z),z\right)$. The coordinates of arbitrary micro-unit Q in the disk with respect to the fixed coordinate system are $\left(x_Q,y_Q,z_Q\right)$.The coordinates of arbitrary micro-unit D in the blade with respect to the fixed coordinate system are $\left(x_D,y_D,z_D\right)$.

1.1.2 Energy equations

The expression of velocity is then obtained by derivation of the time variant coordinates (displacements). Considering the translational motion and the rotation around the z-axis, the total kinetic energy of the shaft can be obtained by integrating the kinetic energy of the micro-unit along the shaft:

$$T_s = \frac{1}{2}\rho_s A_s \int_0^s (\dot{u}_x^2 + \dot{u}_y^2) dz + \frac{1}{2}\rho_s I_{sp} \int_0^s (\Omega + \dot{\phi})^2 \, \mathrm{d}z \tag{1}$$

where S is the length of shaft, ρ_s denotes the density, A_s is the area of shaft cross section, I_{sp} is the polar moment of inertia and $I_{sp} = \int_{A_s} r^2 dA = \frac{\pi}{2} r_s^4$.

the total potential energy of shaft can be given as follows [33,34]:

$$U_s = \frac{1}{2} EI_{sx} \int_0^s \left(\left(\frac{\partial^2 u_x}{\partial z^2} \right)^2 + \left(\frac{\partial^2 u_y}{\partial z^2} \right)^2 \right) \mathrm{d}z + \frac{1}{2} G_s I_{sp} \int_0^s (\frac{\partial \phi}{\partial z})^2 \, \mathrm{d}z \tag{2}$$

where E_s and G_s are Young's modulus and shear modulus, respectively. I_{sx} is the area moment of inertia on the x_1-axis and $I_{sx} = \int_{A_s} y^2 dA = \frac{\pi}{4} r_s^4$.

In this paper, the disk is assumed to be a rigid body without considering its elastic deformation. so the disk cannot be treated as particles. The translational and rotational kinetic energy of the disk is:

$$T_d = \frac{1}{2}\rho_d h_d \int_{r_1}^{r_2} \int_o^{2\pi} \left(\dot{x}_Q^2 + \dot{y}_Q^2 + \dot{z}_Q^2 \right) r \, \mathrm{d}r \, \mathrm{d}\theta \tag{3}$$

In the same way, the kinetic energy associated with the i^{th} blade can be obtained as follows:

$$T_{bi} = \frac{1}{2}\rho_b A_b \int_0^L \left(\dot{x}_D^2 + \dot{y}_D^2 + \dot{z}_D^2 \right) \mathrm{d}l \tag{4}$$

Where A_b is the area of blade cross section, and the total kinetic energy of the disk is:

The bending and centrifugal potential energy of the i^{th} blade can be given as follows [33]

$$U_{bi} = \frac{1}{2} EI \int_0^L (\frac{\partial^2 v_i(l,t)}{\partial r^2})^2 \, \mathrm{d}l \tag{5}$$

1.1.3 Assumed modes

The assumed mode method is adopted to discretize the continuous system. The displacements of shaft can be expressed as following:

$$u_x(z,t) = \mathbf{U}^T \mathbf{q}_x = \mathbf{q}_x^T \mathbf{U} \tag{6}$$

$$u_y(z,t) = \mathbf{U}^T \mathbf{q}_y = \mathbf{q}_y^T \mathbf{U} \tag{7}$$

$$\phi(z,t)=\boldsymbol{\Phi}^{T}\mathbf{q}_{\phi}=\mathbf{q}_{\phi}^{T}\boldsymbol{\Phi} \tag{8}$$

where $\mathbf{U}$ and $\boldsymbol{\Phi}$ denotes the assumed modal matrix, $\mathbf{q}_{x}$, $\mathbf{q}_{y}$, $\mathbf{q}_{\phi}$ denote the generalized coordinate associated with the shaft,

In the similar way, the displacements of blades can be expressed as follows

$$v(l,t)=\mathbf{V}^{T}\mathbf{q}_{v}=\mathbf{q}_{v}^{T}\mathbf{V} \tag{9}$$

where $\mathbf{V}$ denotes the assumed modal matrix associated with the blade, $\mathbf{q}_{v}$ denote the generalized coordinate of the blade.

1.1.4 Discrete vibration equation

Substitution of the above equations into the energy expressions and employment of the Lagrange equations yields the following discretizated equations of motion in matrix notation as

$$\frac{d}{dt}\left(\frac{\partial L}{\partial\dot{\boldsymbol{\eta}}}\right)-\frac{\partial L}{\partial\boldsymbol{\eta}}=\mathbf{Q} \tag{10}$$

$$L=T-U=T_{s}-U_{s}+\sum_{j=1}^{n}T_{dj}+T_{Bj}-U_{Bj} \tag{11}$$

where $\boldsymbol{\eta}$ denotes the generalized coordinate matrix, $\mathbf{Q}$ is the generalized force matrix corresponding to the generalized coordinates. The discretized equations of motion in matrix notation can be given as:

$$\mathbf{M}\ddot{\boldsymbol{\eta}}+\mathbf{C}\dot{\boldsymbol{\eta}}+\mathbf{K}\boldsymbol{\eta}=\mathbf{Q} \tag{12}$$

1.2 Modeling of aerodynamic force

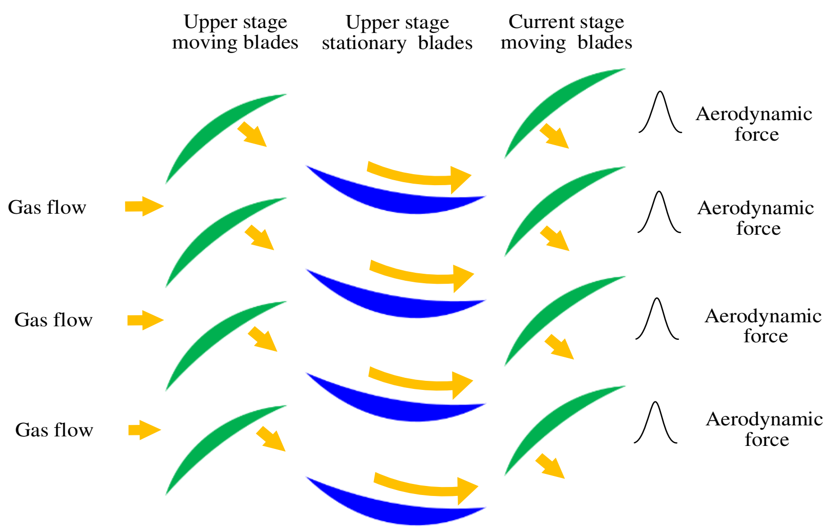

Figure 4: Schematic diagram of aerodynamic force between moving blade and stationary blade

The working mode of the blade disk rotor system is compressed gas or driven by gas. As shown in Figure 4, according to the working principle of the blade disk rotor system, each time the moving blade passes through a stationary blade, it will be coupled with the gas flow through the upper stationary blade, to form a pulse aerodynamic force on the moving blade.

Based on the principle of Fourier decomposition, the pulse signal can be decomposed into the superposition of sinusoidal signals with the pulse frequency as the fundamental frequency. Therefore, the aerodynamic force on the moving blades v_i caused by the gas of the upper stationary blade can be qualitatively modelled as:

$$f_{v_i}(l,t) = p_0 + \sum_{K_j=1}^{K_j} p_{K_j} \sin(K_j N_s \Omega t + \varphi_i) \tag{13}$$

where: p_0 ——Constant component; p_{K_j} ——components of the K_j -th frequency; K_j—— Order of frequency and K_j=1,2,3,4; φ_i ——Initial phase of the i-th blade; $N_s\Omega$ ——fundamental frequency of pulse; N_s——Number of stationary blades.

1.3 Modeling of blade crack's stiffness parameters excitation

Under the action of centrifugal stress caused by rotation and bending vibration caused by aerodynamic force, breathing effects appear on the contact surface of crack as shown in Figure 5, so as to change the stiffness of the cracked blade transiently. Therefore, the stiffness parameter excitation arises in the system.

The method adopted to model the cracked blade is from our recent publication [35]. In the modeling of the cracked blade, the released energy associated with the crack is considered as follows:

$$U_c = \frac{1}{2}\frac{(EI)^2}{K_{\text{crack}}} \boldsymbol{\eta}^T \boldsymbol{V}(l_c)'' \boldsymbol{V}(l_c)''^T \boldsymbol{\eta} \tag{14}$$

where K_{crack} is the breathing stiffness of the crack, depending on the vibration response (bending stress σ_b) and the centrifugal effect (centrifugal stress σ_d). The breathing function is:

$$K_{\text{crack}} = k_c \times \begin{cases} \infty & \sigma_b \geq \sigma_d / y_c \\ \left(\dfrac{h/2 - y_c}{y_0 - y_c}\right)^3 & \sigma_d \Big/ \left(h/4 + y_c/2\right) < \sigma_b < \sigma_d / y_c \\ 1 & \sigma_b \leq \sigma_d \Big/ \left(h/4 + y_c/2\right) \end{cases} \tag{15}$$

where k_c is the stiffness of the open crack, and $k_c = \dfrac{EI}{6(1-\mu^2)hQ(\gamma)}$, γ denotes the relative crack depth [36]

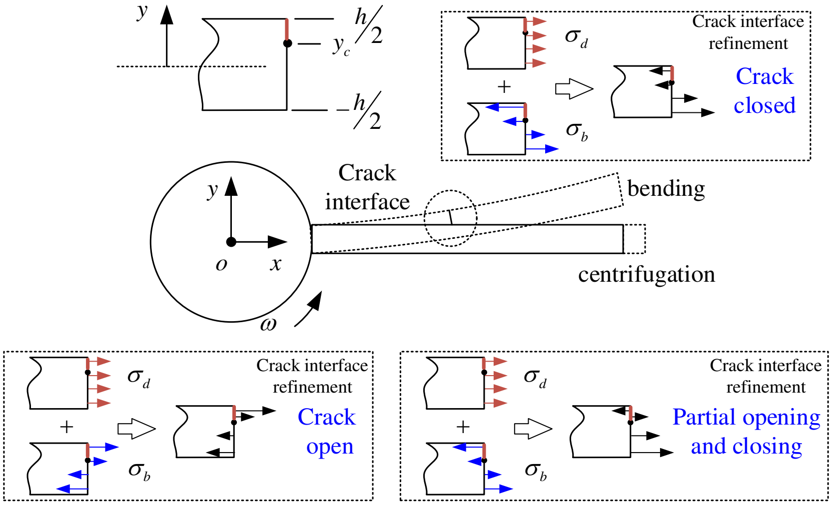

Figure 5: Schematic diagram of crack breathing in rotating blade.

2. Numerical analysis of response characteristics

Based on the dynamic model, special case studis for two structural forms of moving and stationary blades are explored by numerical solution, to intuitively present the expression of typical response characteristics under aerodynamic force and crack stiffness parameter excitations.

2.1 Response characteristics of Synchronous excitation

In the typical simplified system with five stationary blades (N_s=5) and five moving blades (N_d=5), the five moving blades excited by the aerodynamic force synchronously (Synchronous excitation).

This paper focuses on the qualitative study of the characteristics and mechanism under aerodynamic load and crack excitation. Therefore, only the frequency components of transverse vibration and torsional vibration are compared and analyzed.

Considering the inevitable eccentricity of the system, the load forms studied in this section include: eccentricity (Ecce), aerodynamic force (AeroF), crack and aerodynamic force (Crack+AeroF), crack, eccentricity and aerodynamic force (Crack+Ecce+AeroF).

2.1.1 Transverse vibration response

Figure 6 shows the frequency spectrums of the transverse vibration responses. In this case, the rotation speed is 2900RPM, the corresponding rotation frequency ω =48.3Hz (1x)。

As shown in Figure 6 (a), the eccentricity will lead to the rapid increase of the amplitude corresponding to 1x frequency component in the transverse vibration response.

As can be seen in Figure 6 (b), when the system only under the exciting of aerodynamic force, without eccentricity and crack excitations, the amplitude of transverse vibration response is zero, indicating that the resultant force of each aerodynamic forces on transverse vibration is zero.

Under the excitation of aerodynamic force, each blade has bending vibration. Due to the breathing effect of cracks, the bending vibration of the cracked blade is different from that of other blades, resulting in the mistuning of the vibration coupling effect of the blades on the shaft. As shown in Figure 6 (c), under the coupling action of the crack and aerodynamic force, the amplitude of frequency components such as 1x = 48 Hz, 4x = 194 Hz and 6x = 291 Hz increases, where 1x is rotation frequency ω, 4x is $(N_b+1)\omega$, 6x is $(N_b-1)\omega$, and N_b=5.

In transverse vibration, the eccentricity often dominates the vibration response, the amplitude of 1x frequency is very large, the response characteristics under the couping of crack and aerodynamic force are easy to be submerged, as shown in Figure 6 (d). However, qualitatively, the characteristics caused by the coupling of crack and aerodynamic force are different from that of the eccentricity.

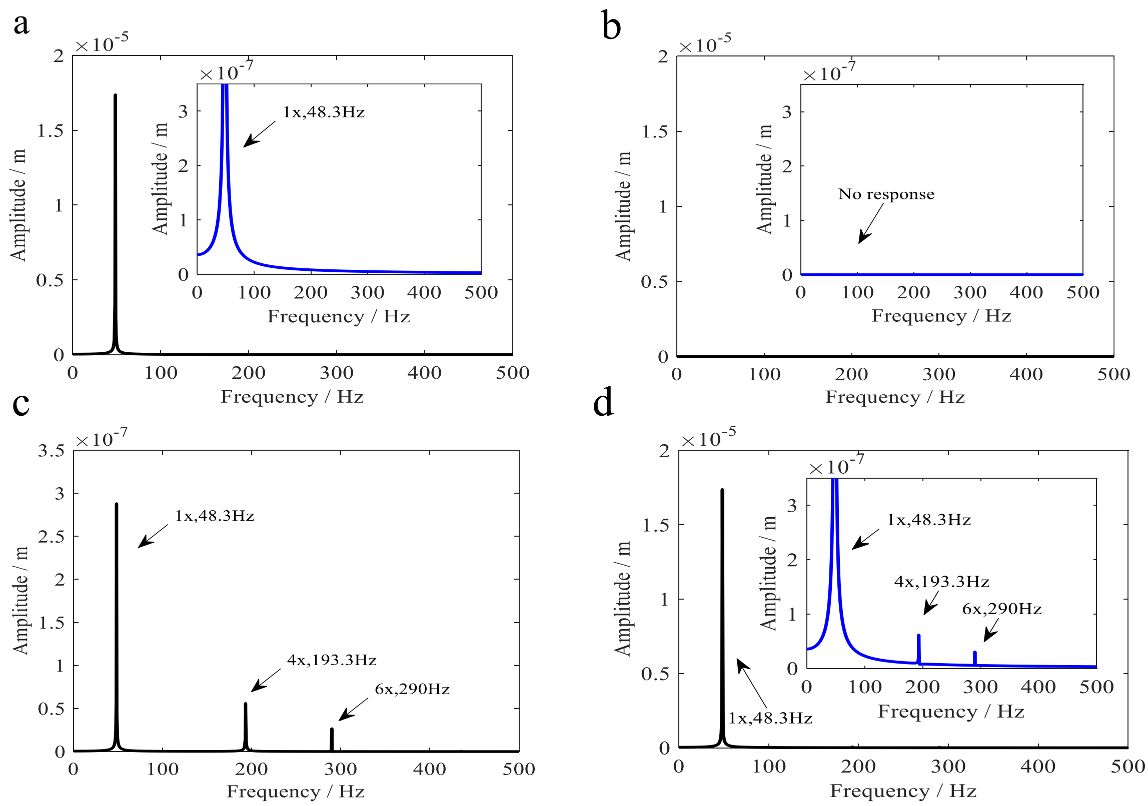

Figure 6: Spectrums of transverse vibration response (N_s=N_d=5). (a) Ecce. (b) AeroF. (c) Crack+AeroF. (d) Crack+Ecce+AeroF.

2.1.2 Torsional vibration response

Figure 7 shows the frequency spectrums of the torsional vibration responses.

As can be seen in Figure 7, in this case, the amplitude of torsional vibration caused by bending-torsion coupling effects is very small, and it is difficult to identify the frequency components of coupled torsional vibration caused by eccentricity in the spectrum of torsional vibration response.

As shown in Figure 7, under the excitation of aerodynamic force, the amplitude of frequency components such as 5x=241.7Hz, 10x =483.3Hz and 15x=725Hz increases, where

5x is $N_b\omega$, 10x is $2N_b\omega$ and 15x is $3N_b\omega$.

In this structural form with five stationary blades and five moving blades, the fundamental frequencies of normal and cracked blades are 5x. The crack leads to the increase of the amplitude of 5x frequency component in the torsional vibration response, as shown in Figure 7.

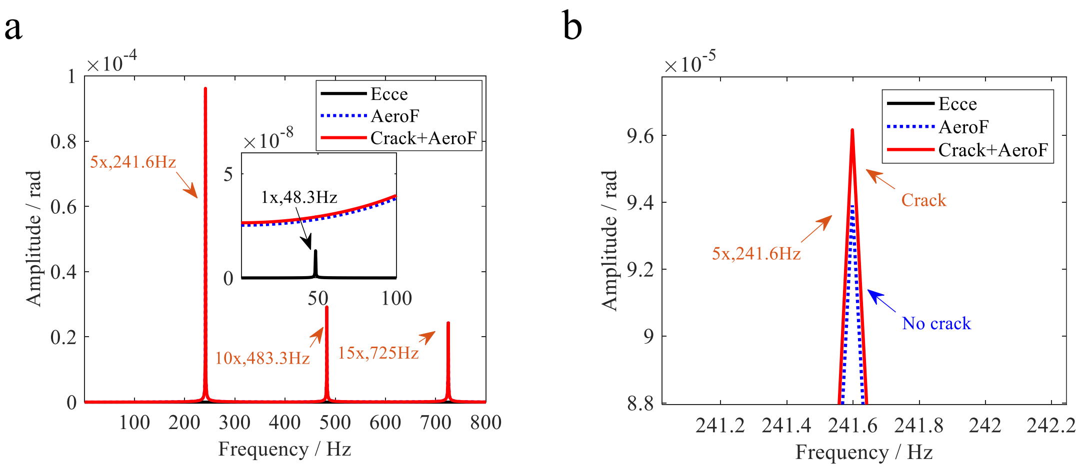

Figure 7: Spectrums of torsional vibration response. (N_s=N_d=5). (a) AeroF. (b) Crack+AeroF.

2.2 Response characteristics of Asynchronous excitation

In the typical simplified system with seven stationary blades (N_s=7) and five moving blades (N_d=5), the five moving blades excited by the aerodynamic force asynchronously (Asynchronous excitation), that is, each moving blade is excited by the aerodynamic force with phase lag.

The transverse vibration responses under asynchronous excitation are shown in Figure 8. There are 15x and 20x frequencies in both normal and cracked systems under aerodynamic force. When there is a crack in the blade, 6x and 8x frequency components appear in the response spectrum, but there is no such frequency component in the normal system.

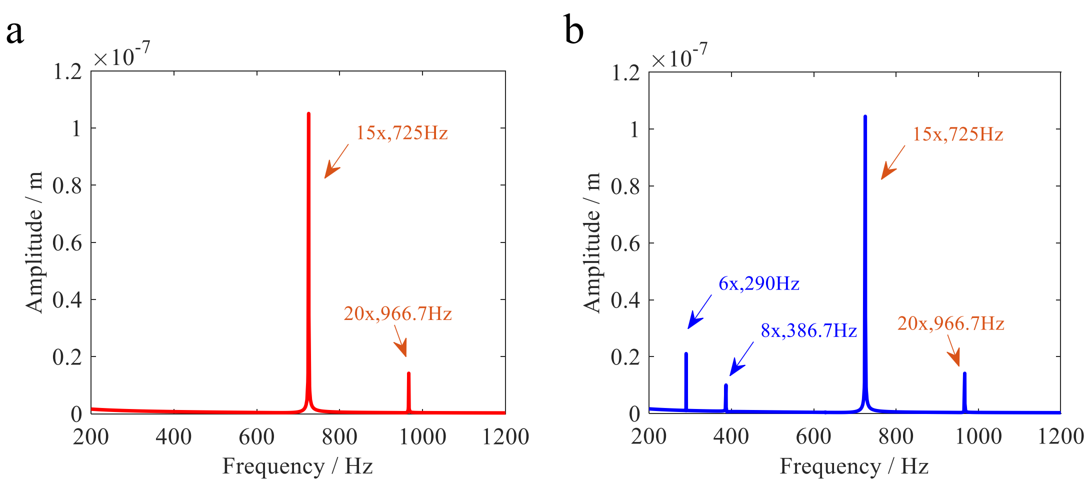

Figure 8: Spectrums of transverse vibration responses (N_s=7, N_d=5). (a) AeroF. (b) Crack+AeroF.

The torsional vibraiton responses are shown in Figure 9. It can be seen from the figure that under the coupling action of aerodynamic force and crack, there are 35x frequency components in both cracked and normal systems, indicating that the response of this frequency component is caused by aerodynamic force. However, the frequency components such as 7x and 14x appear in the cracked system, but not in the normal system. Therefore, this frequency components are caused by the stiffness parameter excitation of the crack.

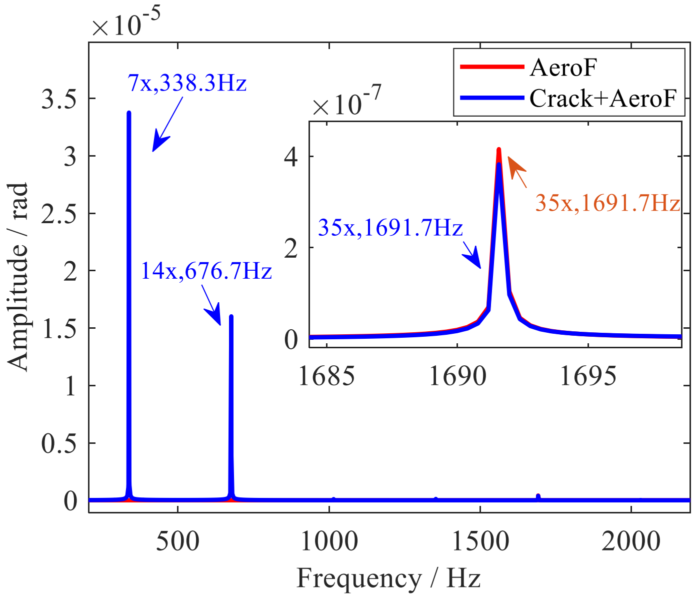

Figure 9: Spectrums of torsional vibration responses (N_s=7, N_d=5).

To sum up, the special case studies based on the dynamic model shows that under asynchronous excitation, the aerodynamic force leads to 15x and 20x frequency components in the transverse vibration response and 35x ($N_s \times N_d \omega$) frequency component in the torsional vibration response. The stiffness parameter excitation of blade crack leads to frequency components such as 6x ($(N_s - 1)\omega$) and 8x ($(N_s + 1)\omega$) in transverse vibration response and 7x ($N_s \omega$) and 14x ($2N_s \omega$) in torsional vibration response. The mechanism will be deduced in detail in Section 4.

3. Mechanism revealing and law explorating of vibration response

The above model based special case studies expounds the basic response characteristics of aerodynamic force and crack excitation. At the same time, it also shows that the structural form will significantly affect the response characteristics.

In this section, from the perspective of kinematics and dynamics, the internal response mechanism of synchronous excitation and asynchronous excitation are revealed firstly, and based on Number Theory, the general law of response characteristics of non coprime forms (synchronous excitation) and coprime forms (asynchronous excitation) are obtained.

3.1 Response Mechanism under Synchronous excitation

Figure 10 is the position relationship of moving and stationary blades during one rotation cycle (N_s=5, N_d=5). In the figure, s_i (i=1,2,3,4,5) are the positions of stationary blades and d_i (i=1,2,3,4,5) are the positions of moving blades.

Figure 11 is the excitation diagram of each moving blade during one rotation cycle, s_i-d_j represents the aerodynamic excitation of the j-th moving blade at the i-th stationary blade. When the numbers of moving and stationary blades are five, during one rotation cycle, due to the airflow at the upper stationary blades, each moving blade is excited by aerodynamic forces at five stationary blades successively, that means the fundamental frequency is $N_s\omega$, and the five moving blades are excited synchronously.

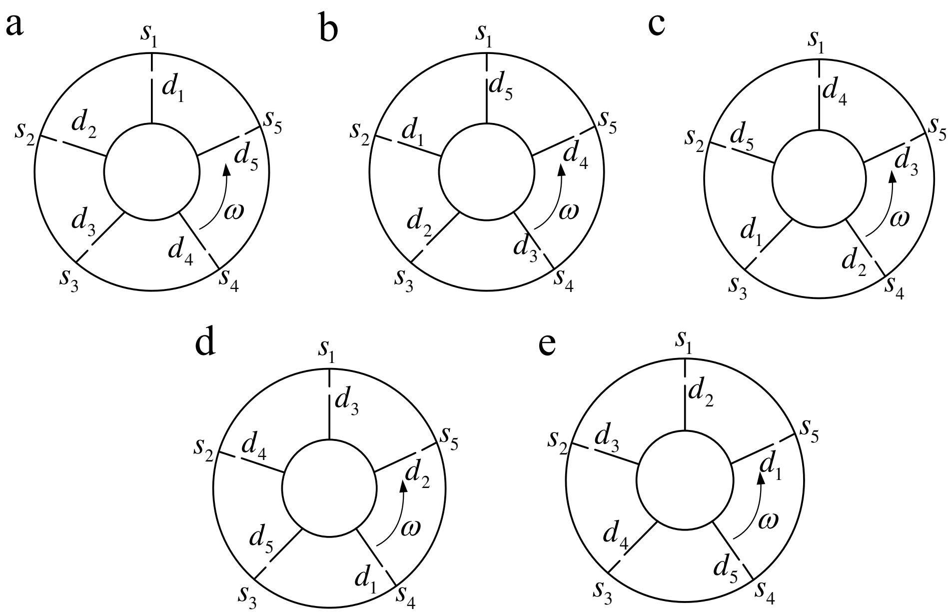

Figure 10: The position relationship of moving and stationary blades during one rotation cycle..(a) 0/5 cycle. (b) 1/5 cycle. (c) 2/5 cycle. (d) 3/5 cycle. (e) 4/5 cycle.

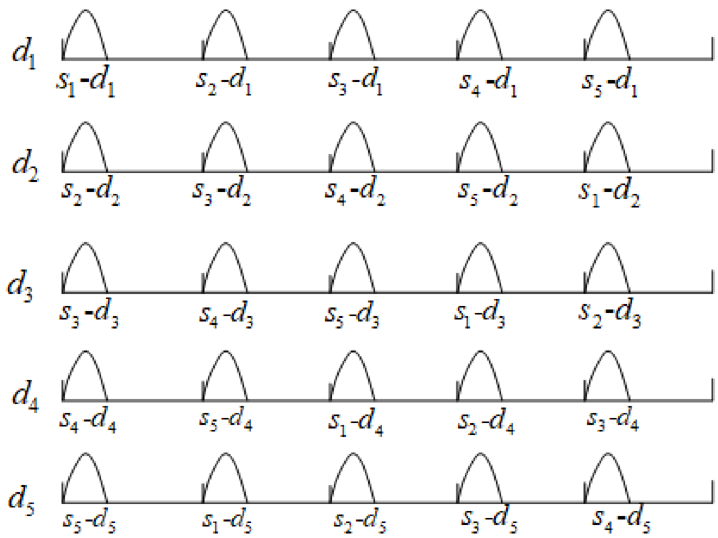

Figure 11: Excitation diagram of each moving blade during one rotation cycle.

3.1.1 Torsional vibration

In the ideal and circularly symmetric blade disk rotor system, the excitation of the torsional vibration of the shaft is the superposition of the excitation torque of each moving blade with the same amplitude, frequency and phase. Therefore, the torsional vibration of the shaft is also equivalent to being excited by a excitation with the fundamental frequency $N_s\omega$, as shown in Figure 12.

This is the mechanism why aerodynamic force causes $N_s\omega$, $2N_s\omega$ and $3N_s\omega$ frequency components in torsional vibration response (shown in Figure 7).

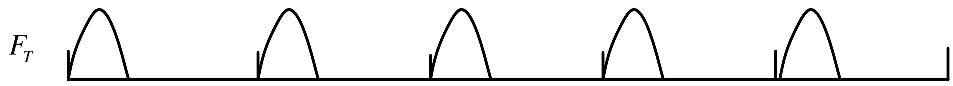

Figure 12: Torsional excitation diagram of shafting during one rotation cycle.

3.1.2 Transverse vibration

The excitation of transverse vibration is the superposition of the transverse components of the excitation of each moving blade. Because the moving blades are circularly symmetrical, the excitation amplitude A of each blade (i=1,2,...,N_d) is equal for the ideal system. Therefore, the excitation of transverse vibration is the superposition of sinusoidal components with uniform phase lag $\left(2\pi/N_d\right)i$, which is satisfied :

$$A\sum_{i=1}^{N_d}\sin\left(\omega t+\frac{2\pi}{N_d}i\right)=0 \tag{15}$$

This is the mechanism why the transverse vibration response amplitude is zero (shown in Figure 6), when under aerodynamic excitation but without crack and eccentric excitation.

When a blade has cracks, its coupling excitation effect on the shafting is different from that of other blades. Therefore, equation (15) is no longer equal to zeros, that is, the superposition of transverse excitation components of each moving blade is no longer zeros.

The mistuning excitation of a blade caused by crack can be qualitatively expressed in the same form as the blade vibration $A\sin\left(K_jN_s\omega t\right)+C$. Moreover, since the cracked blade rotates with the rotating shaft, the transverse component of its mistuning excitation changes with the rotating frequency, which can be expressed as

$$f_c=\sin\left(\omega t\right)\left(A\sin\left(K_jN_s\omega t\right)+C\right) \tag{16}$$

At this time, the transverse vibration has excitation with frequency components ω and $\left(K_jN_s\pm1\right)\omega$, etc.

This is the mechanism why the amplitudes of frequency component such as 1x, $\left(N_b\text{-}1\right)\omega$ =4x , and $\left(N_b+1\right)\omega$=6x increase in transverse vibration under the coupling action of the crack and aerodynamic force, shown in Figure 6.

3.2 Response Mechanism under Asynchronous excitation

This section will study another special case, the response mechanism with seven stationary blades and five moving blades. At this time, each moving blade is excited by aerodynamic load asynchronously (N_s=7, N_d=5).

Figure 13 is the position relationship of moving and stationary blades during $1/N_s$ rotation cycle. In the figure, s_i (i=1,2,3,4,5,6,7) are the positions of stationary blades and d_i (i=1,2,3,4,5) are the positions of moving blades. As can be seen in **Error! Reference source not found.**, during $1/N_s$ rotation cycle, each moving blade is excited once in turn. Moreover, the excitation order of the moving blade is d_1->d_3->d_5->d_2->d_4 ((a)->(b)->(c)->(d)->(e)) and its phase lag is $\left(\left|1/N_s - 1/N_d\right|\right)2\pi$, that is $2\pi/35$.

Figure 14 is the excitation diagram of each moving blade during one rotation cycle, s_i-d_j represents the aerodynamic excitation of the j-th moving blade at the i-th stationary blade. It can be seen from the figure that each moving blade is excited N_s times in one rotation cycle, and the phase lag of each excitation is $2\pi/N_s$.

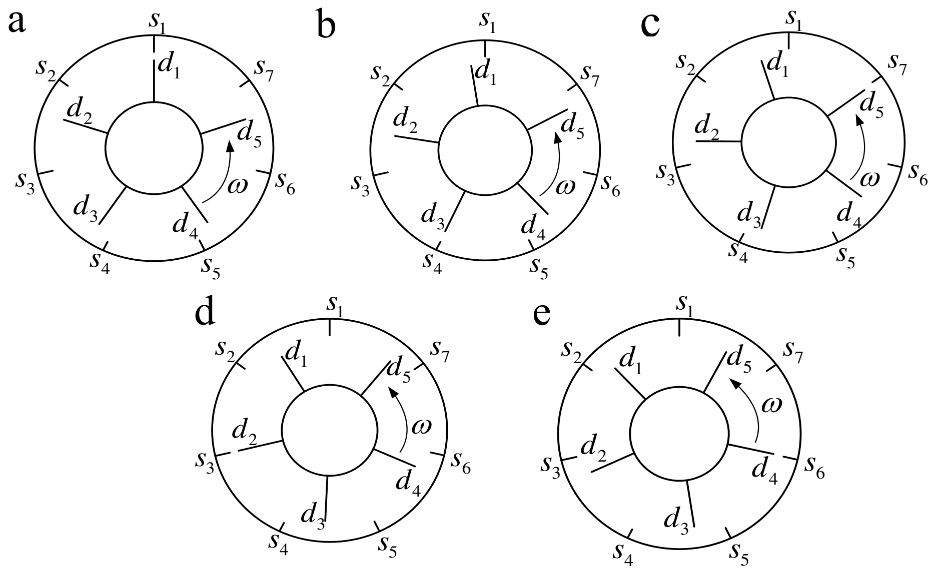

Figure 13: The position relationship of moving and stationary blades during $1/N_s$ rotation cycle.(a) d_1 forced:0/35 cycle. (b) d_3 forced: 1/35 cycle. (c) d_5 forced: 2/35 cycle. (d) d_2 forced: 3/35 cycle. (e) d_4 forced: 4/35 cycle.

Error! Reference source not found.

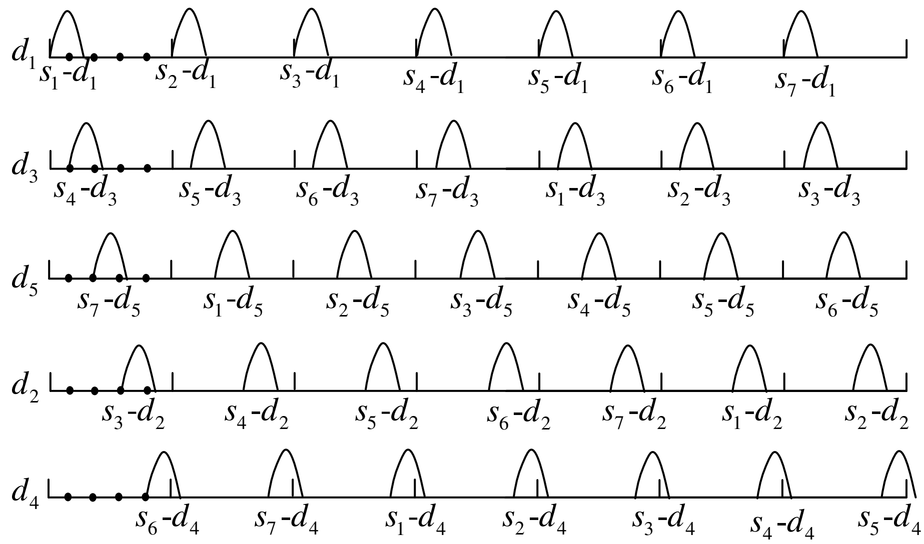

Figure 14: Excitation diagram of each moving blade during one rotation cycle.

3.2.1 Torsional vibration

The excitation transmitted from blade aerodynamic load to torsional vibration is the superposition of aerodynamic pulses with phase lag of each blade, and its schematic diagram is shown in Figure 15. Therefore, the shaft torsional vibration is qualitatively excited by a load with a fundamental frequency $N_s \times N_d$.

Because the lag interval of each pulse can not make each pulse completely independent, but there is an overlapping area between pulses. Therefore, after the superposition of the pulses, the excitation pulsation amplitude decreases and the mean value increases,

Therefore, under the excitation of aerodynamic force, there are components with small amplitude and fundamental frequency of $N_s \times N_d$ in the torsional vibration response. That is the 35x frequency components shown in Figure 9.

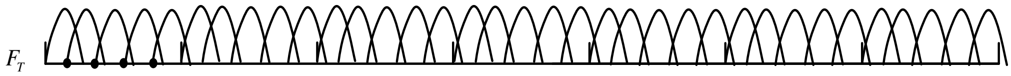

Figure 15: Torsional excitation diagram of shafting during one rotation cycle.

When there is a crack on a blade, the torsional vibration excitation of the cracked blade to the shaft is not consistent with other normal blades, and there is an additional excitation component in torsional vibration caused by the crack mistuning, with the blade vibration frequency $N_s\omega$ as the fundamental frequency. Therefore, under the coupling action of crack and aerodynamic force, 7x and 14x frequency components appear in the torsional vibration response, as shown in Figure 9.

3.2.2 Transverse vibration

The aerodynamic force of each blade will cause excitation on the shaft. It can be seen from Figure 14, the shaft is excited $N_s \times N_d$ times in a rotation cycle, that is, the frequency of excitation is $N_s \times N_d\omega$. With the rotation of the shaft and the change of the excitation position, the transverse component of excitation changes periodically.

As can be seen from **Error! Reference source not found.**, the first excitation is that the moving blade d_1 excited by aerodynamic force at s_1 (**Error! Reference source not found.**(a)), and the second excitation is that the moving blade d_3 excited by aerodynamic force at s_4 (**Error! Reference source not found.**(b)). In this process, the shaft rotates by $\frac{2\pi}{N_s N_d}$ radian and the excitation position of the aerodynamic load rotates by $\frac{3}{N_s}2\pi$ radians (from s_1 to s_4). The position change laws of the subsequent excitation are the same.

Therefore, in this structural form, the change frequency of the excitation position has the following relationship with the shaft rotation frequency

$$\left(\frac{3}{N_s}2\pi\right)\Big/\frac{2\pi}{N_s N_d}=3N_d \tag{16}$$

It shows that the transverse component of aerodynamic force changes with frequency $3N_d\omega$. Therefore, the transverse component of the aerodynamic force can be qualitatively expressed as

$$f_a = A\sin(3N_d\omega t)\left(\sin(N_s \times N_d\omega t)+C\right) \tag{17}$$

By expanding the above formula, it can be seen that the frequency components of transverse excitation are $3N_d\omega$, $(N_s \pm 3)\times N_d\omega$, etc.

This is the mechanism why the amplitudes of frequency component such as $3N_d\omega$=15x and $(N_s\text{-}3)\times N_d\omega$=20x increase in transverse vibration under aerodynamic force, shown in Figure 8.

When there is a crack in a blade, the frequency component of the additional excitation caused by the crack mistuning is the blade vibration frequency $KN_s\omega$, and the of transverse component on the shaft changes with the frequency ω. Therefore, the transverse component caused by crack mistuning can be expressed as $A\sin(\omega t)\left(\sin(KN_s\omega t)+C\right)$.

This is the mechanism why the amplitudes of frequency component such as $(N_s\text{-}1)\omega$ =6x , and $(N_s\text{+}1)\omega$=8x increase in transverse vibration under the coupling action of the crack and aerodynamic force, shown in Figure 8.

3.3 General law of different structural forms

The special case studies of two typical structural forms show that the response characteristics of aerodynamic force and crack misuning and the mechanism of exciting are significantly different under different structural forms. Go a step further, this section will establish the response law of general structural form based on Number theory.

The structural forms can be divided into two categories: the first category, the numbers of moving blades and stationary blades are **coprime**, that is, there is no common divisor other than 1; the second category, the numbers of moving blades and stationary blades are **non coprime**, that is, there is a common divisor other than 1.

3.3.1 Coprime structural form

For a system where the number of moving and stationary blades are coprime, no more than one moving blade is excited by aerodynamic force at any time, and the excitation of each moving blade has phase lag, i.e. asynchronous excitation, such as the typical special case in Section 3.2 and Section 4.2, where $N_s = 7$, $N_d = 5$.

When N_s and N_d are coprime, The general response law can be revealed by

Bézout's identity

If, the integers a and b have the greatest common factor d,

Then, there must be integers i and j, to make ai+bj=d.

According to the above theorem, when N_s and N_d are coprime, their greatest common factor d=1. Therefore, there must be integers i and j to make $N_d j + N_s i = 1$. Considering that i is an arbitrary integer, there must also be an integer i, to make $N_d j - N_s i = 1$.

Divide $N_d N_s$ on both sides of the above formula, and get

$$\frac{j}{N_s} - \frac{i}{N_d} = \frac{1}{N_d N_s} \tag{18}$$

and,

$$\frac{j}{N_s} = \frac{i}{N_d} + \frac{1}{N_d N_s} \tag{19}$$

Multiply 2π on both sides, and get

$$\frac{j}{N_s} 2\pi = \frac{i}{N_d} 2\pi + \frac{1}{N_d N_s} 2\pi \tag{20}$$

The above formula shows that, when N_s and N_d are coprime and the serial number of the coincident moving and stationary blades is set to 0, the angle difference between the i-th moving blade and the j-th stationary blade is $\frac{1}{N_d N_s} 2\pi$.

Therefore, during the rotation of the shaft,the next i-th moving blade can coincide with the next j-th stationary blade passing through $\frac{1}{N_d N_s} 2\pi$ radian and be excited by aerodynamic force.

In this process, the shaft rotates by $\frac{2\pi}{N_s N_d}$ radian and the excitation position of the aerodynamic load rotates by $\frac{j}{N_s}2\pi$ radians. Therefore, the change frequency of the excitation position has the following relationship with the shaft rotation frequency

$$\left(\frac{j}{N_s}2\pi\right)/\left(\frac{1}{N_d N_s}2\pi\right)=N_d j \tag{21}$$

It shows that the transverse component of aerodynamic force changes with frequency $N_d j\omega$. Therefore, the transverse component of the aerodynamic force can be qualitatively expressed as

$$f_a=A\sin\left(N_d j\omega t\right)\left(\sin\left(N_s N_d \omega t\right)+C\right) \tag{22}$$

The excitation transmitted from blade aerodynamic force to torsional vibration is the superposition of aerodynamic pulses with phase lag of each blade. Therefore, the shaft torsional vibration is qualitatively excited by a load with a fundamental frequency $N_s \times N_d$. Therefore, the excitaion of torsional vibration can be qualitatively expressed as $A\sin\left(N_s N_d \omega t\right)+C$.

Specifically, in Section 4.2, when N_s=7 and N_d=5, there are j=3 and i=2, marking

$$\frac{3}{N_s}2\pi=\frac{2}{N_d}2\pi+\frac{1}{N_d N_s}2\pi \tag{23}$$

Therefore, in **Error! Reference source not found.**, the next excitation positions are the next 2-th moving blades (d_1->d_3->d_5->d_2->d_4) passing through the next 3-th stationary blades (s_1->s_4->s_7->s_3->s_6).

3.3.2 Non coprime structural form

For a system where the number of moving and stationary blades are coprime, that is, there is a maximum common divisor m (m≠1) between N_s and N_d . The results show that at any excitation position, there is a group of circularly symmetrical moving blades with a number of m, which are synchronously excited by aerodynamic force.

According to equation (15), the resultant force of the transverse components of a group of cyclic symmetry blades under synchronous excitation is zero. Therefore, under the excitation of aerodynamic force, the response amplitude of non coprime ideal system is zero.

Since the m moving blades are excited at the same time, the torsional excitation of the m blades are superimposed to form a whole excitation. Therefore, in one rotation cycle, the torsional excitation frequency is $N_s N_d \omega/m$. Therefore, torsional excitation can be qualitatively expressed as:

$$F_T=A\sin\left(\left(N_s N_d \omega/m\right)t\right)+C \tag{24}$$

3.3.3 Crack characteristics

When there is a crack in a blade, the frequency component of the additional excitation caused by the crack mistuning is the blade vibration frequency $KN_s\omega$. Therefore, the additional excitation component in torsional vibration caused by the crack mistuningcan be expressed as $\sin\left(KN_s\omega t\right)+C$. Considering that the transverse component of the excitation of the cracked moving blade changes with the frequency ω , the transverse component caused by crack mistuning can be expressed as $A\sin\left(\omega t\right)\left(\sin\left(KN_s\omega t\right)+C\right)$.

Conclusions

From the numerical solution based response characteristic analysis to the kinematics and dynamics based essential response mechanism revealing, from the model based special case study to the Number Theory based general law establishing, the response mechanism of blade disk rotor system under the coupling effects of crack and aerodynamic force is studied comprehensively and deeply. The conclusions are as follows:

(1) For a system in which the numbers of moving blades and stationary blades are coprime, the moving blades are asynchronously excited by the aerodynamic force at each stationary blade, successively. The general form of excitation for lateral vibration by aerodynamic load is $A\sin\left(N_d j\omega t\right)\left(\sin\left(N_s N_d\omega t\right)+C\right)$ and the general form of excitation for torsional vibration by aerodynamic load is $A\sin\left(N_s N_d\omega t\right)+C$.

(2) For a system in which the numbers of moving blades and stationary blades are non coprime (the common divisor is *m*), there are *m* moving blades with cyclic symmetrical distribution excited by aerodynamic force. The excitation superposition result of transverse components of these *m* blades is zero. Therefore, there is no excitation in lateral vibration. The general form of excitation for torsional vibration by aerodynamic load is $A\sin\left(\left(N_s N_d\omega/m\right)t\right)+C$.

(3) When there is a crack in a moving blade, the vibration response of the cracked blade under aerodynamic load is different from that of other blades, and the stiffness parameter excitation of the crack appears. Therefore, the cracked blade will causes new excitation into the torsional vibration and transverse vibration of the system. In torsional vibraton, the amplitudes corresponding to frequency components $K_j N_s\omega$ are increased. In the lateral vibration, new modulation components are produced with the blade vibration frequency as the carrier and the rotation frequency as the modulation source $A\sin\left(\omega t\right)\left(\sin\left(K_j N_s\omega t\right)+C\right)$.

(4) At present, this study only focus on the ideal and circularly symmetric blade disk rotor system, and the inevitable random mistuning is not considered. The complex coupling characteristics and mechanism between mistuned moving blade, mistuned static blade and inherent eccentricity will be discussed in the next paper.

Data Availability

All data generated or analysed during this study are included in this published article.

Conflicts of Interest

The authors declare that we have no conflicts of interests about the publication of this paper.

Acknowledgments

This work was supported by the National Natural Science Foundation of China (Grant No. 51805548), the Natural Science Foundation of Hunan Province China (Grant No. 2020JJ5756), and the Scientific Research Starting Foundation of Central South University (No. 202044013).

Author contributions

Jinsong Yang (Data curation: Equal; Writing – original draft: Lead); **Jingsong Xie** (Conceptualization: Lead; Formal analysis: Lead; Methodology: Lead; Validation: Lead); **Tiantian Wang** (Supervision: Equal; Visualization: Lead); **Fei Yang** (Conceptualization: Supporting; Formal analysis: Supporting; Investigation: Equal; Resources: Lead); **Jinglong Chen** (Conceptualization: Supporting; Formal analysis: Supporting; Resources: Supporting; Supervision: Supporting; Writing – original draft: Equal)

References

[1] R. Ambur, S. Rinderknecht. "Unbalance detection in rotor systems with active bearings using self-sensing piezoelectric actuators," *Mechanical systems and signal processing*, vol. no. 6 2018, 102(MAR.1):72-86.

[2] J. Yao, J. Dai, L. Liu "Unbalanced Vibration Response Reduction of Rotor Using Active Magnetic Actuator Based on PD Control,". 2019.

[3] J. Xie, Y. Zi "Mechanism explanation and experimental verification of a new modulation frequency characteristic in a disturbed crack rotor," *Nonlinear Dynamics*, 2018.

[4] J. Xie, J. Chen, Y. Peng, et al. "A New Concept of Instantaneous Whirling Speed for Cracked Rotor's Axis Orbit," *Applied Sciences*, 2019, 9(19):4120.

[5] C. Liu, D. Jiang "Torsional vibration characteristics and experimental study of cracked rotor system with torsional oscillation," *Engineering Failure Analysis*, 2020, 116:104737.

[6] Z. Li, Y. Li, D. Wang, et al. "Dynamic Characteristics of Rotor System with a Slant Crack Based on Fractional Damping," *Chinese Journal of Mechanical Engineering*, 2021, 34(1):27.

[7] Y. Yang, J. Wang, Y. Wang, et al. "Dynamical analysis of hollow-shaft dual-rotor system with circular cracks" *Journal of Low Frequency Noise Vibration and Active Control*, 2020:146134842094828.

[8] S. Su, H. Cao, Y. Zhang "Dynamic modeling and characteristics analysis of cylindrical roller bearing with the surface texture on raceways," *Mechanical Systems and Signal Processing*, 2021, 158:107709.

[9] L. Zheng, Y. Xiang, C. Sheng “Nonlinear Dynamic Modeling and Vibration Analysis of Faulty Rolling Bearing Based On Collision Impact,” *Journal of Computational and Nonlinear Dynamics*, 2021.

[10] M. Luo, Y. Guo, Andre H, et al. “Dynamic modeling and quantitative diagnosis for dual-impulse behavior of rolling element bearing with a spall on inner race,” *Mechanical Systems and Signal Processing*, 2021, 158(7):107711.

[11] Bachar L, Dadon I, Klein R, et al. “The effects of the operating conditions and tooth fault on gear vibration signature,” *Mechanical Systems and Signal Processing*, 2021, 154(8):107508.

[12] Z. Shen, B. Qiao, Yang L, et al. “Fault mechanism and dynamic modeling of planetary gear with gear wear,” *Mechanism and Machine Theory*, 2021, 155:104098.

[13] Y. Yang, N. Hu, J. Tang, et al. “Dynamic analysis for a spur geared rotor system with tooth tip chipping based on an improved time-varying mesh stiffness model,” *Mechanism and Machine Theory*, 2021, 165:104435.

[14] M. Liu, D. Cao, X. Zhang, et al. “Nonlinear dynamic responses of beamlike truss based on the equivalent nonlinear beam model,” *International Journal of Mechanical Sciences*, 2021, 194(5):106197.

[15] Wu, Nan “Study of forced vibration response of a beam with a breathing crack using iteration method,” *Journal of Mechanical Science and Technology*, 2015, 29(7):2827-2835.

[16] L. Yang, Z. Yang, Z. Mao, et al. “Dynamic Characteristic Analysis of Rotating Blade With Transverse Crack—Part I: Modeling, Modification, and Validation,” *Journal of Vibration and Acoustics*, 2020, 143(5):1-36.

[17] L. Yang, Z. Mao, S. Wu, et al. “Nonlinear dynamic behavior of rotating blade with breathing crack,” *Frontiers of Mechanical Engineering*, 2021(2).

[18] C. Li “Free vibration analysis of a rotating varying-thickness-twisted blade with arbitrary boundary conditions,” *Journal of Sound and Vibration*, 2020, 492.

[19] Shuai, Wang, Yanyang, et al. “Effects of multiple cracks on the forced response of centrifugal impellers,” *Mechanical Systems & Signal Processing*, 2015.

[20] J Joachim, Nyssen F, Batailly A. “Numerical Investigation of a Mistuned Academic Bladed Disk Dynamics with Blade/Casing Contact,” *Journal of Engineering for Gas Turbines and Power*, 2020.

[21] Heydari H, Khorram A, Afzalipour L. “The Influences of Stagger and Pretwist Angles of Blades on Coupling Vibration in Shaft-Disk-Blade Systems,” *Journal of vibration and acoustics*, 2019, 142(1):1-38.

[22] Y. Jin, Z. Liu, Y. Yang, et al. “Nonlinear vibrations of a dual-rotor-bearing-coupling misalignment system with blade-casing rubbing,” *Journal of Sound and Vibration*, 2021, 497(6):115948.

[23] B. Li, H. Ma, X. Yu, et al. “Nonlinear vibration and dynamic stability analysis of rotor-blade system with nonlinear supports,” *Archive of Applied Mechanics*, 2019, 89(7):1-28.

[24] J. Zeng, C. Zhao, M. Hui, et al. “Dynamic Response Characteristics of the Shaft-Blisk-Casing System with Blade-Tip Rubbing Fault,” *Engineering Failure Analysis*, 2021(3):105406.

[25] N. Wang, C. Liu, D. Jiang, et al. “Casing vibration response prediction of dual-rotor-blade-casing system with blade-casing rubbing,” *Mechanical Systems and Signal Processing*, 2019,

118(MAR.1):61-77.

[26] C. Ma, L. Liu, L. Gang, et al. “Transient Dynamic Response of the Aero-Engine Dual-Rotor System Under the Blades Loss Load,” *Springer*, Singapore, 2018.

[27] H. Zhang, T. Zhao, H. Zhang, et al. “Dynamic characteristics of mistuned bladed disk system under rub-impact force,” *Advances in Mechanical Engineering*, 2020, 12(11):168781402097306.

[28] Z. Li, T. Zhao, H. Kou, et al. “Vibration Characteristics of Multi-Stage Blade–Disk–Shaft Integrated Structure with Three-Dimensional Crack,” *Journal of Vibration Engineering & Technologies*, 2020:1-15.

[29] H. Ma, F. Yin, Z. Wu, et al. “Nonlinear vibration response analysis of a rotor-blade system with blade-tip rubbing,” *Nonlinear Dynamics*, 2016, 84(3):1225-1258.

[30] H. She, C. Li, Q. Tang, et al. “Influence mechanism of disk position and flexibility on natural frequencies and critical speeds of a shaft-disk-blade unit,” *Journal of Sound & Vibration*, 2020:115156.

[31] J. Xie, J. Liu, J. Chen, et al. “Blade damage monitoring method base on frequency domain statistical index of shaft’s random vibration,” *Mechanical Systems and Signal Processing*, 2022, https://doi.org/10.1016/j.ymssp.2021.108351

[32] J. Yang, J. Xie, G. Chen, et al. “An efficient method for vibration equations with time varying coefficients and nonlinearities,” *Journal of Low Frequency Noise, Vibration and Active Contro*l, 2021, https://doi.org/10.1177/14613484211025151

[33] M. Wu, S. Huang “On the vibration of a cracked rotating blade,” *Shock and Vibration*, 1998. **5**(5-6): 317-323.

[34] Y. Chiu ,S. Huang “The influence of a cracked blade on rotor's free vibration,” *Journal of Vibration and Acoustics-Transactions of the ASME*, 2008. **130**(5):054502.

[35] J. Xie, Y. Zi, M. Zhang, et al. “A novel vibration modeling method for a rotating blade with breathing cracks,” *SCIENCE CHINA Technological Sciences*, 2019, 62(02):163-178.

[36] B. Huang and J. Kuang “Effect of a local crack on the dynamic characteristics of a rotating grouped blade disc,” *Proceedings of the Institution of Mechanical Engineers Part C-Journal of Mechanical Engineering Science*, 2002. **216**(4): 447-457.